# Probabilistic initial orbit determination and object tracking in cislunar space using passive radio frequency sensors

**Dr. Erin Griggs, Matt Schierholtz, Dr. Islam Hussein, Mark Bolden, Kyle Charles, and Dr. Holly Borowski**

*Trusted Space, Inc.*

## 1. ABSTRACT

In this paper we build on the work we presented at the 2022 AMOS Conference [1]. In that work, we focused on the processing of optical observations from spacecraft orbiting in Cislunar space. Specifically, we (a) extended the use of Probabilistic Admissible Region (PAR) that was developed for near-Earth Initial Orbit Determination (IOD) to the cislunar environment using only a single short arc optical measurement, and (b) implemented the Particle Gaussian Mixture Filter (PGMF) for the processing of subsequent optical observations of the target in an integrated framework. This integrated PAR-PGMF solution was shown to be a rigorous initial orbit determination and filtering framework that is scalable, robust to modeling errors and large IOD uncertainties, and to be able to handle multi-modal uncertainties and highly nonlinear and chaotic dynamical systems that are present in the cislunar regime.

In this paper, we shift our attention to passive radio frequency (RF) observations. We will focus on Time Delay of Arrival (TDOA) and One-Way Doppler (OWD) measurement types. Specifically, given an uncertain initial orbit using the PAR technique, we will use the PGMF to process subsequent passive RF observations of the target for orbit determination. Moreover, we will explore scenarios where optical data of the target is also available. We will study the performance of the PAR-PGMF framework under two alternative scenarios: 1) only passive RF data is used to perform PGMF orbit determination, and 2) optical and passive RF data are fused to perform PGMF orbit determination. In both of these scenarios, we will use electro-optical data to perform the PAR orbit initialization. We will compare the performances from these two scenarios against the optical-only scenario, as described in [1]. While we anticipate improved PAR-PGMF performance with the inclusion of RF data, we will also assess the degree of improvement that RF data adds to the processing of optical data only.

## 2. INTRODUCTION

Cislunar initial orbit determination (IOD) and orbit determination (OD) are quickly becoming operational challenges for the United States Space Force (USSF). As one of the five core competencies of the USSF Spacepower Doctrine, securing and protecting this region of space is a high priority [2]. Spacecraft that transit through this space, however, are often only opportunistically detected, and can go for days and weeks on end without observation. The complex dynamics introduced by the Earth/Moon gravity system can allow for cislunar spacecraft to enter and exit conventional orbit regimes, such as Geosynchronous (GEO) and Low-Earth Orbit (LEO), unexpectedly. To ensure safe operations in all orbit regimes, it is necessary to monitor and attribute spacecraft in the cislunar domain.

In this paper, we build off of our 2022 AMOS Conference paper [1]. There it was demonstrated that the combination of Probabilistic Admissible Region (PAR) and Particle Gaussian Mixture Filter (PGMF) techniques enabled IOD and OD in the cislunar regime. Due to the colossal distances of the environment, observations of an object are usually condensed to a short arc or single observation point. To rapidly generate an uncertain trajectory for object tracking, high-fidelity probabilistic IOD techniques, such as the PAR approach [3], are needed. Such techniques complement the single observation with other hypothesized information (e.g., target albedo-area product that correlates with range to the object from the sensor location) to generate a probabilistic representation of the object's orbit. Once an orbit is initialized, subsequent tracking of a cislunar object also presents us with additional unique challenges. We first note that, as is the case with IOD in Earth orbit, the resulting initialized orbit is typically multi-modal [3]. Any subsequent object tracking technique must therefore be able to handle multi-modal object state uncertainties. On top of that, the cislunar domain is subject to highly nonlinear, possibly chaotic dynamical behavior. It is therefore desired to develop and implement high-fidelity nonlinear filters that can accommodate multi-modal probability distributions, chaotic bifurcations, and that are robust to modeling errors. One advanced algorithm that is capable of handling all of these challenges is the PGMF [4, 5]. The PGMF combines the best of the

two worlds of particle filtering (specifically, its propagation step) and the Gaussian Mixture Model (GMM) form of the Unscented Kalman Filter (UKF) (specifically, its nonlinear update step) [6].

In [1], we incorporated electro-optical (EO) observations of right ascension (RA) and declination (DEC) to update the information state after particle propagation in the PGMF. When available, EO measurements provide good observability to the target. EO is not always available, though, as it is frequently limited by weather, solar, and lunar exclusions. Passive radio frequency (RF) data is a complementary source of observations to EO but has been underutilized in the past for orbit determination state updates. Active RF techniques, such as radar or two-way ranging, are common techniques used to track spacecraft throughout the solar system. For example, the Deep Space Network (DSN) still implements two-way RF ranging to the Voyager spacecraft to track their progress to interstellar space [7]. Radar and two-way ranging techniques, however, alert or require cooperation from the target spacecraft of the tracking activities. Passive RF only "listens" for serendipitous transmission from target spacecraft. These opportune messages come with high uncertainties, and in the past, have been seen to corrupt orbit determination results when used in tandem with EO. Here, we acknowledge those uncertainties, but claim that we can use passive RF to improve the knowledge of information state in the PGMF, complementary to EO. Furthermore, on its own, passive RF can be available during solar and lunar exclusions, through weather, and at ranges that extend beyond what is detectable by an optical system. The fundamental measurements are the time and frequency at which a signal is received by an observer, and as with EO, passive RF systems can detect signals without attribution.

Using passive RF for orbit determination is fundamentally challenging because we typically do not know *when* an uncooperative satellite is transmitting. The range between the target and observer is derived from the exact transmit and receipt times of the signal and can be wildly incorrect with just a small error in either of these terms. This classic problem is solved in RF navigation systems, like the Global Positioning System (GPS), by the use of high precision timing systems, both onboard the satellites and within the control segment on the ground. A common sense of time is maintained and distributed to the users through the GPS ephemeris message, which has an explicit message structure that all GPS receivers identify and track [8]. Without this common time reference and message structure, as with a typical passive RF sensing system, only the time at which the signal is received is known. Another challenge of passive RF is that the exact transmission frequency of the signal is typically unknown. For uncooperative targets, we can only assume that the satellite transmits its messages at common or protected frequencies (e.g., S-band, X-band, Ka-band, etc.), but these frequency bands often span many millions of hertz. Additionally, the transmit frequency is affected by the Doppler shift induced by the relative motion between the transmitter and receiver, target and receiver clock biases, and the target transmitting hardware.

We believe and will show in this paper that PAR-PGMF is capable of overcoming the challenges associated with passive RF data ingestion. As described in [1], we start with orbit initialization of a cislunar spacecraft via a single RA/DEC observation using the PAR technique (details of the PAR IOD concept from the 2022 AMOS paper are described in Section 4.1). From this initial information state, we use the PGMF to determine future states through propagation and state update steps. We use both EO and passive RF observations independently as well as when they are fused together in the PGMF for orbit determination of the cislunar target. Specifically for passive RF, we use Time Difference of Arrival (TDOA) from three ground stations and One-Way Doppler (OWD) from up to three ground stations derived from time and frequency measurements. We demonstrate the utility of passive RF data, both on its own and fused with EO measurements through the following cases: 1) OD on a cislunar target with only EO data, 2) OD for the same target with a combination of TDOA and OWD observations from combinations of up to three ground stations, and finally, 3) EO fused with TDOA and OD observations for OD of the cislunar target. All cases utilize the PAR with a single EO observation to determination the IOD state. We compare the entropy and percent errors of position and velocity of the estimated state of the cislunar target by the EO, RF, and fusion of EO and RF, and assess the improvement and utility that passive RF observations provide to a cislunar OD system.

In summary, in this paper we: 1) demonstrate a baseline case that uses the PAR to initialize an orbit of a satellite in the cislunar domain from a single EO observation, 2) implement the PGMF for the processing of passive RF observations of the target, and 3) make comparisons of performance of the OD tool using EO-only, RF-only, and a fusion of EO-RF observations. We demonstrate the PAR-PGMF is a complete IOD and filtering framework that is capable of cislunar object orbit initialization and tracking with multiple phenomenologies.

## 3. TECHNICAL CHALLENGES

As described in [1], approaches to IOD/OD in the cislunar domain must solve the following challenges. First, due to the large distances between the observers and target objects, there is typically insufficient data and knowledge to initialize an orbit. Orbit initialization requires at least six independent parameters to be able to solve for the six-dimensional state of the target object. With the very long distances, the object, however, moves slowly relative to the observing sensor. This implies that even for an extended period of time, observations of the object contain too little independent information to initialize an orbit. For optical sensors, for example, this means that we effectively only have two parameters (e.g., azimuth and elevation from an EO sensor), which is four fewer than the needed six variables to determine the orbit of the object. This implies that other parameters, such as the object's orbital energy and albedo area product, need to be hypothesized, as opposed to being directly measured.

Second, there is uncertainty in the hypothesized and measured variables for initializing an orbit. This uncertainty translates into an uncertain orbit when the observed and hypothesized quantities are mathematically mapped during orbit initialization. When properly performed in a probabilistic fashion, the uncertainty in the initialized orbit is typically multi-modal. Intuitively, this results from the fact that with short arc angles-only data, for example, it is typically unclear which direction the object is traveling. This results in two modalities in the initial PAR. A Gaussian distribution model, while it simplifies the object tracking process, introduces assumptions that are easily violated in highly non-linear dynamical systems, such as in the cislunar domain. Therefore, it is important to retain the non-Gaussian, multi-modal nature of the initialized uncertain orbit.

Finally, the dynamics of the cislunar domain are inherently nonlinear. This means that even very small errors or mismodeling of the uncertainty can result in very large deviations between where the object really is going and where the algorithm believes it is going. This will result in losing track of the object. Traditional quasi-Gaussian nonlinear filtering approximations, such as the UKF [6], cannot handle non-Gaussian filtering problems. They are, however, powerful for their computationally tractable uncertainty update step when a measurement of the target is obtained –an observation that we will return to when we discuss the PGMF later in the paper. For non-quasi-Gaussian techniques such as the Particle Filter (PF) [9], the curse of dimensionality reveals itself in the form of particle depletion, which we will discuss more in Section 4.2.

Current approaches to IOD/OD will, however, typically fail at addressing at least one of these challenges, resulting in a failure to initialize an orbit and/or losing the object altogether. The main reason for this is that existing tools used for space object IOD/OD typically assume two-body dynamics and perturbations thereof that do not apply to the three-body dynamics nature in the cislunar domain. For example, the Constrained Admissible Region (CAR) approach described in [10] requires specification of ranges on parameters such as semi-major axis and eccentricity, and employ the physics of the unperturbed two-body (Earth-spacecraft) system. Orbits in the cislunar domain, however, have no notion of semi-major axis or eccentricity, and clearly do not evolve according to two-body dynamics. While a technique such as the PAR was also developed for two-body systems, it is extensible to the cislunar domain as was shown in [1] and in this paper.

## 4. TECHNICAL SOLUTION

### 4.1 Astrometric-Radiometric PAR Initialization for IOD

In this paper we use a single electro-optical astrometric observation and radiometric techniques to initialize an uncertain trajectory for an object in cislunar space. After that we use the PGMF to perform OD for a number of EO only, OWD only, TDOA only, and combinations thereof. The core idea of the PAR technique is to map the measurements and their uncertainties along with any information about complementary variables using a sampling-based approach to representing the target's uncertain state. It is a probabilistic IOD technique that is in contrast with deterministic single trajectory IOD approaches. Deterministic approaches to IOD generate a single track for an object. Because they generate only a single trajectory, deterministic techniques are typically very sensitive to sensor noise and other assumptions made about the object's orbit, especially for nonlinear and chaotic regimes such as cislunar. Unlike deterministic IOD approaches, methods such as the CAR and the PAR generate a family of orbits around the object's true orbit using the observed measurement from the sensor. When performed in a probabilistically rigorous way, the generated family of orbits are guaranteed to encompass the true orbit of the object. With every additional observation of the target after orbit initialization, the family of orbits, also called the

"particle cloud" for simplicity, converge towards the true object orbit if the subsequent OD method is robust and unbiased.

The PAR approach starts with the single sensor observation. The PAR technique can be tailored to any sensor phenomenology. However, in this paper, we will use an optical observation framework. Given an observation and the sensor noise standard deviation, PAR proceeds by sampling a large number, $N$, of simulated observations. The more the number of samples, the higher the fidelity of the PAR procedure in modeling the uncertainty of the object's orbit. The number of particles is only limited by the processing and memory of the available computational resources, and by any limits on meeting tactical mission timelines. For each sample, we need four additional independent parameters to generate a corresponding full orbit sample.

Our approach first takes advantage of the light intensity measured by the optical sensor. This provides a third direct observable parameter that provides information on the range to the target. We emphasize here that use of light intensity is only for the PAR, and not for the PGMF in subsequent orbit determination updates for the electro-optical set of scenarios we use to demonstrate our approach later in this paper. Using the light intensity along with the associated noise statistics, one can then generate $N$ light intensity sample points. Since the first three parameters, two angles (i.e., azimuth and elevation) and a light intensity, are independent, we can then solve for the object's positional information uniquely, first using the equation of a diffuse/specular sphere to compute range:

$$M_v = -26.74 - 2.5\log(A\rho[\beta F_1(\varphi) + (1-\beta)F_2(\varphi)]) + 5\log R$$

where

$$F_1(\varphi) = \frac{2}{3\pi^2}[(\pi - \varphi)cos\ \varphi + \sin\varphi]$$

$$F_2(\varphi) = \frac{1}{4\pi}$$

and where $M_v$ is the visual magnitude of the observed object, $A\rho$ is the albedo area product, $\varphi$ is the solar phase angle, $\beta$ is the sample mixing coefficient, and $R$ is the range from the observer to the object [11]. Here we denote $F_2$ as a function of solar phase angle by convention. For other shapes there is a solar phase angle dependence to this term. The visual magnitude is sampled based on the uncertainty of the radiometric measurement. The albedo area product is sampled uniformly across all spacecraft possibilities. The range of solar phase angles is sampled uniformly and can be significantly constrained by combining the angles data with the maximum allowable range based on the cislunar domain definition. Given the line of sight, the solar phase angle is very insensitive to $R$ within the domain. This process provides a range to the target for each sample. The approach enables the technique to work with no knowledge of object material or size. The result is large uncertainty in range that is constrained by independent measurements. Using angles and range we can convert to relative positions from the sensor to the target:

$$x_{ot} = R\cos(AZ)\cos(EL)$$
$$y_{ot} = R\sin(AZ)\cos(EL)$$
$$z_{ot} = R\sin(EL)$$

where $AZ, EL$ are the observed angles, $x_{ot}, y_{ot}, z_{ot}$ are the positional cartesian coordinates from the sensor to the target, and $R$ is the range from the sensor to the target.

We then need three additional independent variables that give us information on the object's velocity. For these, we use known limits on the sensor's maximum angular rates (i.e., azimuth and elevation rates) to bound the maximum rate an object can move within the sensor's frame for the object to be detected by the sensor. See Fig. *1*. If the object moves any faster than that across the sensor field of view, we know that the sensor cannot, by definition, detect it. This provides two hypothesized (since they are not directly measured) independent parameters. The final bound we can hypothesize is the object's speed. For cislunar, we take advantage of the equation governing the object's velocity and the Jacobi integral for the circular restricted three-body problem (CR3BP) [12]:


$$\dot{AZ} = \sum_{i=0}^{n} Rand[0, \frac{Max\ Streak}{Exposure\ Duration}]$$

$$\dot{EL} = \sum_{i=0}^{n} Rand[0, \frac{Max\ Streak}{Exposure\ Duration}]$$

Fig. 1. Maximum Streak Length Detectable

$$\dot{x}^2 + \dot{y}^2 + \dot{z}^2 = (x^2 + y^2) + 2\left(\frac{1-\mu}{r_{13}}\right) + \frac{2\mu}{r_{23}} - C$$

where $\dot{x}, \dot{y}, \dot{z}$ are the cartesian velocity components of the target, $x, y$ and $z$ are the cartesian position components, $\mu$ is the non-dimensional mass of the moon, $r_{13}$ is the range from earth to the object, $r_{23}$ is the range from the moon to the object, and $C$ is the Jacobi constant. The CR3BP approximation of the more complex three-body dynamics governing the cislunar domain introduces relatively small errors that will be corrected with a subsequent robust OD method such as the PGMF, which we will discuss later in this section. *This equation is the equivalent of using the energy equation in the CAR and PAR to hypothesize an object's orbital semi-major axis for the two-body problem.*

The Jacobi integral equation is only one equation with three unknowns (the cartesian components of velocity). We complete the system of three equations by taking the derivative of the relationship between angles and the observer and target positions to get the following two equations:

$$\dot{AZ} = \frac{(cos\, AZ)^2}{(x_t - x_o)}[\dot{y}_t - \dot{y}_o + (\dot{x}_o - \dot{x}_t)tan\, AZ\,]$$

and

$$\dot{El} = \frac{(cos\, El)^2}{\sqrt{(x_t - x_o)^2 + (y_t - y_o)^2}}[\dot{z}_t - \dot{z}_o - tan\, El\frac{(x_t - x_o)(\dot{x}_t - \dot{x}_o) + (y_t - y_o)(\dot{y}_t - \dot{y}_o)}{\sqrt{(x_t - x_o)^2 + (y_t - y_o)^2}}]$$

$$\dot{El} = \frac{(\cos El)^2}{\sqrt{(x_t - x_o)^2 + (y_t - y_o)^2}}[\dot{z}_t - \dot{z}_o - \tan El\frac{(x_t - x_o)(\dot{x}_t - \dot{x}_o) + (y_t - y_o)(\dot{y}_t - \dot{y}_o)}{\sqrt{(x_t - x_o)^2 + (y_t - y_o)^2}}]$$

where $x_o, y_o, z_o$ are the position terms of the observer, $x_t, y_t, z_t$ are the position terms of the target, $\dot{x}_o, \dot{y}_o, \dot{z}_o$ are the velocity terms for the observer velocity, $\dot{x}_t, \dot{y}_t, \dot{z}_t$ are the velocity terms for the target velocity, $AZ$ and $EL$ are the measured angles, and $\dot{AZ}$, and $\dot{EL}$ are the constrained angle rates. The above three equations (the Jacobi equation and the two angle rate equations) are independent and can thus be used to solve for the three velocity components.

While the above equations seem to be nonlinear in the unknown velocity components, we note here that the angle rate equations are linear in the three unknown velocity variables. In these two equations, one can solve for two of the components, say the $\dot{x}_t$ and $\dot{y}_t$ velocity components, in terms of the third variable $\dot{z}_t$ velocity component, and then replace the occurrence of $\dot{x}_t$ and $\dot{y}_t$ in the Jacobi integral equation to get a single equation that is quadratic in $\dot{z}_t$. We then solve for $\dot{z}_t$ given the hypothesized values for the Jacobi constant and the angle rates. Given the value for $\dot{z}_t$, we can then obtain the solution for $\dot{x}_t$ and $\dot{y}_t$. With this we have a particle cloud with each particle having all six state variables (three position and three velocity) fully solved for.

We note here the quadratic nature of the equation in $\dot{z}_t$. This implies that there are two solutions for the cartesian velocity components. This results in the bimodal nature of the uncertainty cloud mentioned in Section 0. This bimodality refers to the fact that when using angles and range information, we do not have any information on velocity (i.e., travel direction). This ambiguity results in the two modes in the initialized PAR. Thus, the resulting cloud of orbits for the object that represent its orbital uncertainty will not be Gaussian. Another contributing factor to the non-Gaussian nature of the resulting PAR is the fact that while the angles and range are typically Gaussian in nature, angle rates and the Jacobi constant uncertainties are assumed to be uniform. This mix of Gaussian and uniform uncertainties are mapped through the various nonlinear geometric and Jacobi integral equations to solve for the state are highly nonlinear algebraic equations. That will result in a complex, multi-modal, and non-Gaussian distribution in the object's state uncertainty. We note here that the PAR process is embarrassingly parallelizable. For example, for $N = 10{,}000$ particles, on an industry-standard laptop, the particle cloud is generated from a single observation in about 70 milliseconds without optimizing the code that generates the cloud. With optimized code and advanced onboard processors, far more particles can be generated in less time to generate a higher fidelity representation of the target's orbital uncertainty. We will seek to understand the trade space balancing between the number of particles against the available onboard computations in future research

### 4.2 PGMF for Uncertainty Reduction and Object Custody

In this section we describe the PGMF approach to OD. For a full demonstration of the PGMF for optical cislunar OD, please see [1]. PGMF was shown to be a robust approach for tracking objects in the cislunar domain due its ability to handle non-Gaussian uncertainties and errors introduced by the PAR (e.g., CR3BP assumption) during initial orbit determination. Here, we briefly describe the general PGMF technique and its advantages.

As discussed earlier in the paper when describing electro-optical PAR, uncertainty is non-Gaussian and multi-modal. Moreover, post orbit initialization, in the chaotic three-body system bifurcations can occur. For orbit determination, the main challenge for current techniques is that highly nonlinear nature of the dynamics combined with the non-Gaussian nature of uncertainty generated from the PAR. Traditional quasi-Gaussian nonlinear filtering approximations, such as the Kalman Filter (KF) and the UKF [6], cannot handle non-Gaussian filtering problems. They are, however, powerful for their computationally tractable uncertainty *update* step when an observation of the target is obtained. The curse of dimensionality reveals itself in the form of particle depletion in the PF [9], where the initial uncertainty is in the form of a particle cloud generated from the IOD step that is then propagated and updated in a Bayesian framework whenever a new observation of the target is obtained. Particle depletion is the phenomenon where in the PF update step particles with very low likelihood of being close to the truth are removed, resulting in effectively a very small number of particles near the true state of the target. This, in turn, may result in a loss of the object's true track, especially for highly non-linear and chaotic dynamical systems where particle abundance and diversity become crucial. We note, however, that otherwise the PF is powerful for *propagation* of uncertainty for nonlinear, possibly chaotic, systems and is highly parallelizable.

While above we noted the reasons why popular nonlinear methods such as the UKF and the PF will fail for tracking objects in the cislunar domain, we have highlighted their strengths since the PGMF combines the powers of both methods and yet avoids their flaws. The PGMF is a robust approach that can handle the non-Gaussian nature of the particle cloud and that is robust to errors introduced into the PAR process such as the use of the CR3BP assumption, as well as other errors introduced in the subsequent uncertainty propagation. The PGMF was originally developed by Raihan and Chakravorty in Refs. [4, 5]. With the object's orbit probabilistically initialized using the PAR, presented as a non-Gaussian cloud of orbital particles, the PGMF performs OD on that cloud as subsequent observations of the target are received. Referring to Fig. 2, the PGMF is kicked off by first propagating the particle cloud using the dynamical equations governing the cislunar domain. This propagation is performed to the time when the next observation of the target arrives, at which point we convert the propagated particle cloud into a GMM by clustering the particles using a clustering algorithm such the k-means++ [13] or the Expectation Maximization algorithm (EM) [14]. A UKF update step is then performed on the propagated prior GMM analytically to obtain the posterior GMM. The observable here can be optical angles-only observations or passive RF TDOA or OWD observations, or combinations thereof in a multi-phenomenology fusion frame, as will be demonstrated later in the paper. With the GMM updated, one then samples this posterior GMM to obtain a new particle cloud that is then propagated to the time when the next observation is obtained. This process is repeated for all subsequent observations collected by the sensor(s).

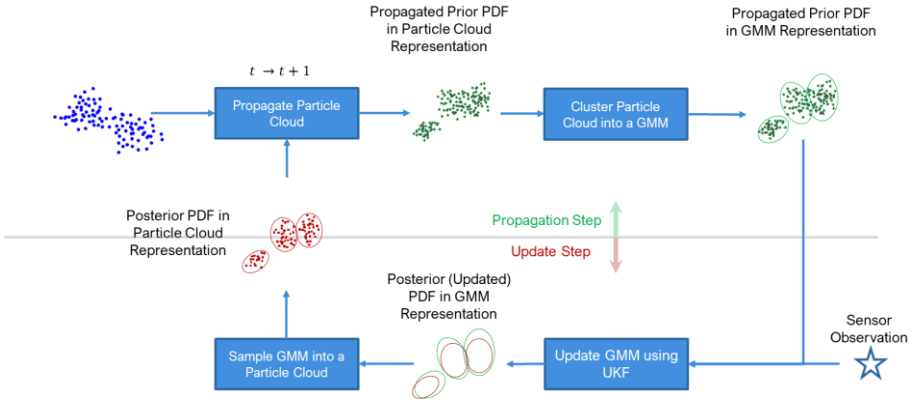


Fig. 2. PGMF Approach

As can be seen, the PGMF is essentially based on the PF except for the updated step where an observation updated GMM is used to resample the cloud. A key factor that makes the PGMF attractive is that every operation described in Fig. 2 is scalable, rendering the entire algorithm scalable. This is because the PGMF uses the UKF GMM update step, which is *computationally tractable*. In our simulation studies of the PGMF, it was found that the update step is

far less computationally expensive than the propagation step. For propagation, the PGMF takes advantage of the *embarrassingly parallelizable* particle filter's propagation of uncertainty for nonlinear, possibly chaotic, systems step. Furthermore, the PGMF is immune to the "curse of dimensionality" due to the clustering-based UKF GMM update step that results in resampling all particles so that they are all located near the true orbit as measured using the sensor observation. As such, the PGMF allows us to get the best of the two worlds of the GMM-based UKF (analytical, nonlinear, and scalable update step) and the PF (nonlinear and scalable propagation step), while avoiding the shortcomings of both. Finally, the PGMF is robust to modeling errors (see [4, 5] for details) due to the particle nature at the heart of the approach. This is important for nonlinear and chaotic dynamical systems where slight modeling errors can result in loss of custody of the target. Robustness also implies that we can use simpler physical models for the dynamics and yet be able to maintain custody of the target. This is key to being able to keep the software lightweight with small computing and power requirements, especially when used for on-orbit IOD/OD. In the use cases shown later in the paper, this robustness quality enabled us to use simplified propagation that are crude approximations of the ground truth models used to generate the data ingested by the PGMF. The PGMF (propagation and update) was able to process data at rates as high as 1000 times faster than real-time.

### 4.3 Passive RF Observations

In this paper, we expand our PGMF implementation from [1] to incorporate passive RF observations to the update step. This requires that we have relationships that relate the state of a PGMF particle in the particle cloud back to OWD and TDOA measurements. These observables are derived from two RF measurements received by the observing ground site $s_i$: the *time*, $t_{s_i}$, at which the signal is received at ground station *i*, and the *absolute frequency*, $f_{s_i}$, of the signal at receipt at ground station *i*. We relate the time and frequency of signal receipt to range and range rate with two fundamental equations:

$$t_{s_i} - t^* = \frac{r_i}{c} = \frac{\sqrt{(x_t - x_i)^2 + (y_t - y_i)^2 + (z_t - z_i)^2}}{c}$$

$$f_{s_i} = \left(1 - \frac{\dot{r}_i}{c}\right) f^* = \left(1 - \frac{\sqrt{(\dot{x}_t - \dot{x}_i)^2 + (\dot{y}_t - \dot{y}_i)^2 + (\dot{z}_t - \dot{z}_i)^2}}{c}\right) f^*$$

where $x_t, y_t, z_t$ and $\dot{x}_t, \dot{y}_t, \dot{z}_t$ are the position and velocity terms for the target velocity, $x_i, y_i, z_i$ and $\dot{x}_i, \dot{y}_i, \dot{z}_i$ are the position and velocity terms of the $i^{\text{th}}$ ground station receiving the RF signal, $c$ is the speed of light in vacuum, $t^*$ is the target time of signal transmission, and $f^*$ is the original transmission frequency. These relationships have dependencies on $t^*$ and $f^*$, both of which are typically uncertain for a cislunar target.

To remove the dependency on $t^*$, we use the common RF tracking technique, TDOA, to take differences in the receipt time from sets of two spatially diverse ground sites [15]:

$$TDOA_{i,j} = \left(t_{s_i} - t^*\right) - \left(t_{s_j} - t^*\right) = t_{s_i} - t_{s_j}$$

For a set of three ground sites, we assign a primary ground station, $s_1$, and subtract from it the time of arrival of the same signal at two other ground stations to create two TDOA measurements, $TDOA_{1,2}$ and $TDOA_{1,3}$. All ground sites must be in view of the target to receive the same signal and make the TDOA measurement, but a greater spatial diversity of sites enables a more unique set of time difference values to enhance observability.

These two TDOA measurements are related to the ranges between the target and ground sites in the following relationships.

$$c * TDOA_{1,2} = c * (t_1 - t_2) = r_1 - r_2$$
$$c * TDOA_{1,3} = c * (t_1 - t_3) = r_1 - r_3$$

where $r_1$, $r_2$, and $r_3$ are the ranges between the target and ground sites $s_1$, $s_2$, and $s_3$, respectively. TDOA eliminates the need for absolute knowledge of the original transmit time of the signal, $t^*$, from the target; however, in this paper, we make a few simplifications to be addressed in future work. First, we assume that the received passive RF signal can be distinguished at a specific point in time for each of the ground stations (e.g., as in a pulse, or known

message structure in the signal sequence). This is to synchronize the signal time of arrival and frequency as the same signal at each of the ground stations. We also assume the collection ground sites are synchronized to a common timing reference, eliminating the need to model receiver clock biases in the TDOA measurements. Finally, we assume that the signal experiences no atmospheric delays –i.e., geometric differences between the transmitter and each receiver are the only cause for differences in the signal time of flight.

The observed frequency, $f_{s_i}$, is directly related to the target's relative range rate to the ground site, $\dot{r}_i$, with a dependency on the transmission frequency, $f^*$. In this paper, we make the assumption that the target transmission center frequency, $f^*$, is known for the OWD observations, but we allow for a lack of certainty around that central frequency. For many cooperative targets, transmission frequency bands are published by the International Telecommunication Union (ITU) and Federal Communications Commission (FCC) [16, 17]. Knowledge of the transmission frequency for uncooperative targets, however, is more uncertain.

For OWD, multiple ground stations are not required to update the target's state, but as we use three stations for the TDOA measurement, we also process OWD measurements from up to three ground sites, with results detailed in Section 5.2. As we will show in our analysis, any number or combination of TDOA and OWD observations can be used to provide an update to the target's information state.

## 5. RESULTS & ANALYSIS

To assess our approach, we demonstrate the PAR-PGMF against a representative cislunar trajectory. The true trajectory used for these simulations is a lunar resonant reflection orbit, with a resonance of three with the Moon (P/3). Its course over one lunar orbit is plotted in Fig. *3* in the Earth-Moon Body Barycentric Rotating (EMBBR) frame in a General Mission Analysis Tool (GMAT) simulation.

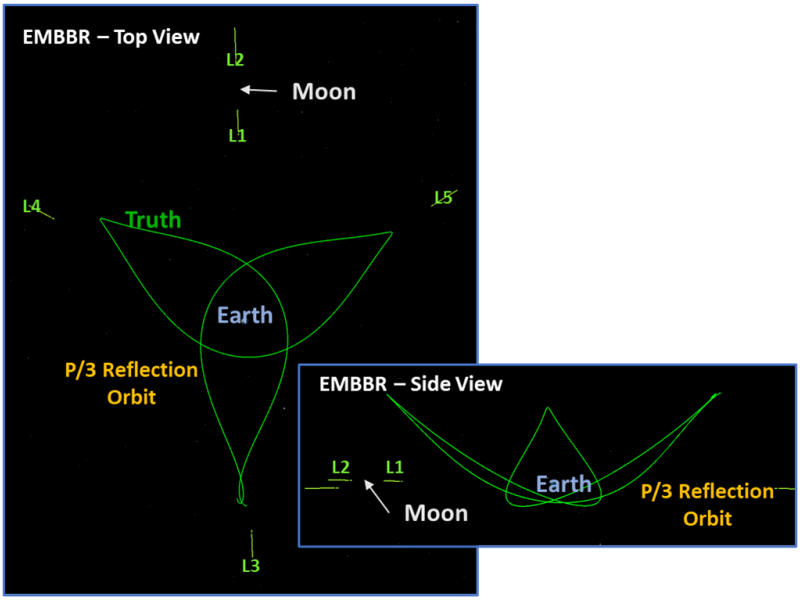


Fig. 3. P/3 Lunar Resonant Reflection Orbit, EMBBR Frame from zenith and ecliptic directions.

The first two views above show the object's trajectory for nearly a month, however, we limit our simulation time to focus on a single target pass over a series of grounds sites. Fig. 4 provides a focused view of the limited part of the trajectory used for the following simulation runs. This short portion of the orbit begins far above the ecliptic at nearly lunar distance from the Earth. The target's trajectory brings it closer to Earth, with all observations made while the spacecraft's distance from Earth is decreasing. Our simulation includes three ground-based observers assumed to be located in Maui, Midway, and Marshall Islands, with their sensor characteristics described in Table 1.

Table 1. Locations and Phenomenologies of Ground-Based Observers

| Name | Latitude (°) | Longitude (°) | Altitude (m) | Phenomenology |
|---|---|---|---|---|
| Maui | 20.7 | -156.3 | 3058 | EO and RF |
| Midway | 28 | -177.4 | 4 | RF only |
| Marshall Islands | 11.6 | 165.3 | 2 | RF only |

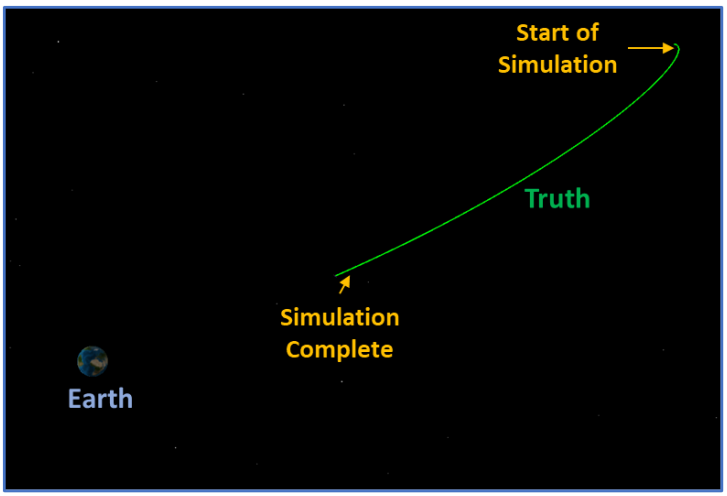

Fig. 4. P/3 Lunar Resonant Reflection Orbit, EMBBR Frame. First Four Days of Propagation Shown.

In propagating the particle cloud for each step, the PGMF uses an Orekit propagator. This is configured with Earth as a central attractor, with a gravity field of degree and order 12. The Sun, Moon, and Jupiter are modeled as point masses and added to the perturbing forces, along with Solar Radiation Pressure (SRP). The position tolerance, for numerical integration purposes, is 0.1 m. The truth simulation, on the other hand, uses a degree and order of 36 for the gravity field, a position tolerance of 0.001 m and adds an atmospheric drag force model. The measurements generated by the truth simulation include Gaussian sensor noise.

There are three use cases the authors simulated for orbit determination: EO only, RF only, and EO-RF Fusion. All of these use an initial PAR information state generated with a single EO observation. There is only one type of EO measurement used (AZ, EL), but RF has two types of measurements that were explored. The first is OWD, which was simulated with one, two, and three ground stations reporting independent Doppler shift values. The second is TDOA, which requires a minimum of three ground stations to report the received time of a signal from the spacecraft. We demonstrate eight combinations of these measurements to simulate:

- EO only,
- TDOA only,
- One-, two-, and three-station OWD,
- TDOA with one-station OWD,
- TDOA with three-station OWD, and
- all three phenomenologies, EO with TDOA and three-station OWD, fused together.

To evaluate the performance of the PGMF simulation in producing a representative particle cloud, true error of position and velocity were used. To assess the overall uncertainty within the particle cloud at each time step, a sample of particles is taken, and their entropy is calculated. Higher entropy means there is a greater diversity of particle states, which means less certainty. An entropy comparison of the eight simulations is presented at the end of this section.

### 5.1 EO Only

Using only EO observations, the results are as follows in Fig. 5.

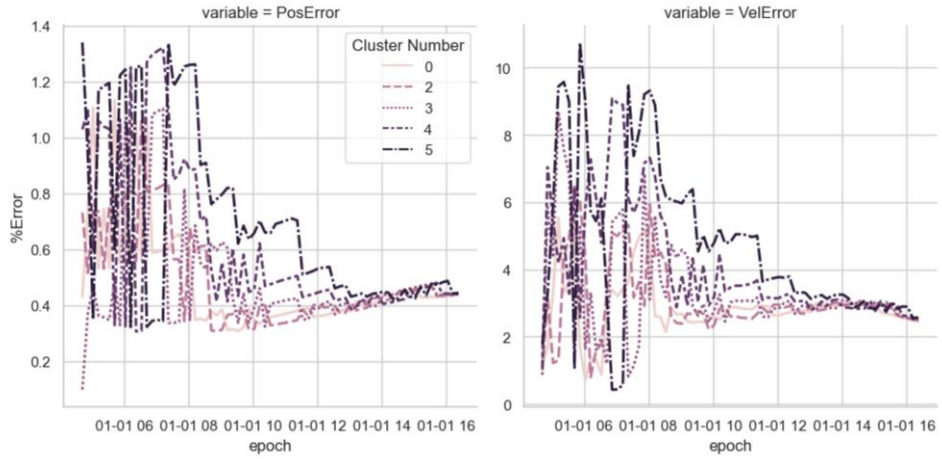


Fig. 5. Position and Velocity Errors for EO-Only Observations

The above plot, and all following error plots, show the average percent error of five GMM clusters for the PGMF update step. This simulation, and all subsequent simulations, shows 16 hours of observation time.

For this particular case of EO measurements only, initialized with an EO PAR, the average position error starts with a large spread around about 0.8%, then quickly converges down to about 0.45% as more measurements are processed. The average velocity error starts with a spread between 1% and 10%, but the cluster averages converge and are continuing to decrease as the simulation ends. Given more time, as seen in previous work by these authors, the position and velocity errors will continue to decrease [1].

Since the scales involved are so large, the range of the spacecraft is approximately 3,000,000 km, so a one percent error in position corresponds to a position error of about 3,000 km. For velocity, the magnitude of the state is about 700 m/s, so a one percent error corresponds to 7 m/s. These error values ae provided for context and are not the exact values.

## 5.2 RF Only

### 5.2.1 Single-Station OWD

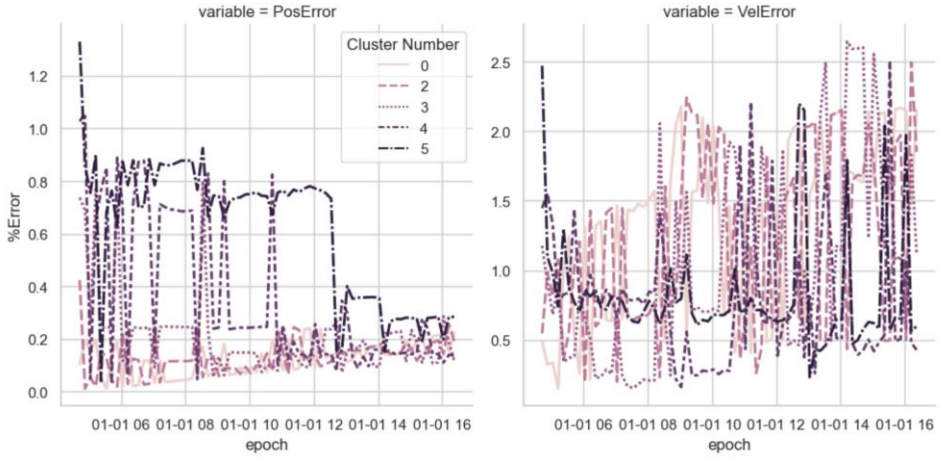


Fig. 6. Position and Velocity Errors for Single-Station OWD (1OWD)

While the average position error results from the single-receiver OWD case (shown in Fig. 6) is quite low (0.2% on average near the end), the velocity error remains high and highly variable over the course of the simulation. This denotes a large variance in the particle cloud, which can also be seen in the entropy comparison plot in a following section.

This result is quite significant, as it shows that the PGMF can perform OD with OWD measurements from a single ground station. This is a very commonly available form of data, so it is useful in an abundance of scenarios.

### 5.2.2 Two-Station OWD

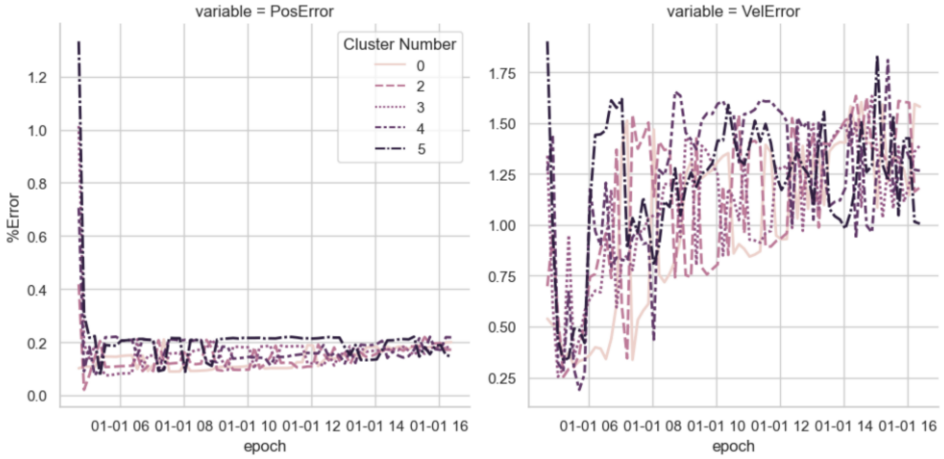


Fig. 7. Position and Velocity Errors for Two-Station OWD (2OWD)

The average percent position error results shown in Fig. 7 for the Two-Station One-Way Doppler (2OWD) case start out much lower on average than those of the 1OWD case but end the simulation in a similar converging error state. The velocity error results are better (smaller and with less spread). As might be expected, this shows that two OWD stations are better than one. The entropy plot (later) shows slightly lower entropy and faster convergence, which agrees with the results here.

### 5.2.3 Three-Station OWD

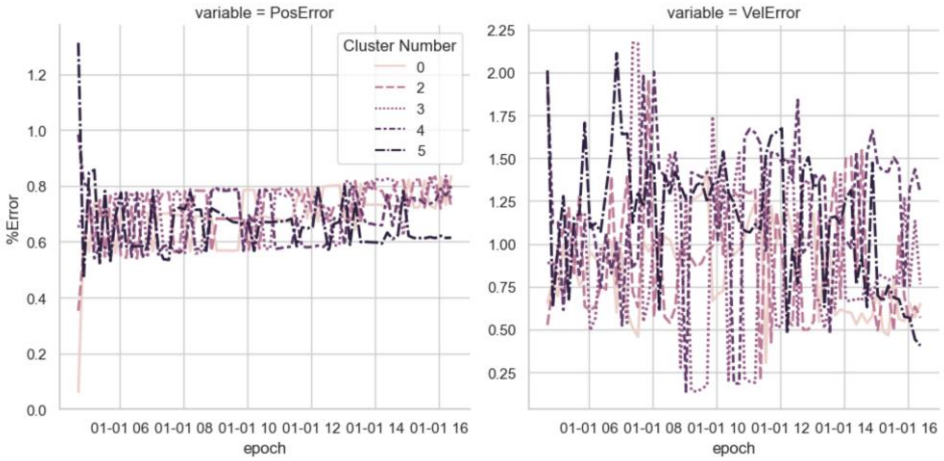


Fig. 8. Position and Velocity Errors for Three-Station OWD (3OWD)

The average percent position error results shown in Fig. 8 for Three-Station One-Way Doppler (3OWD) are higher than those for 1OWD or 2OWD. However, the velocity error results are smaller and have less variance. Over time this leads to small position errors. Additionally, as seen in the entropy plot in Section 5.4, the entropy for this case is lower than those cases with fewer ground stations. This is in line with expectations.

### 5.2.4 Three-Station TDOA

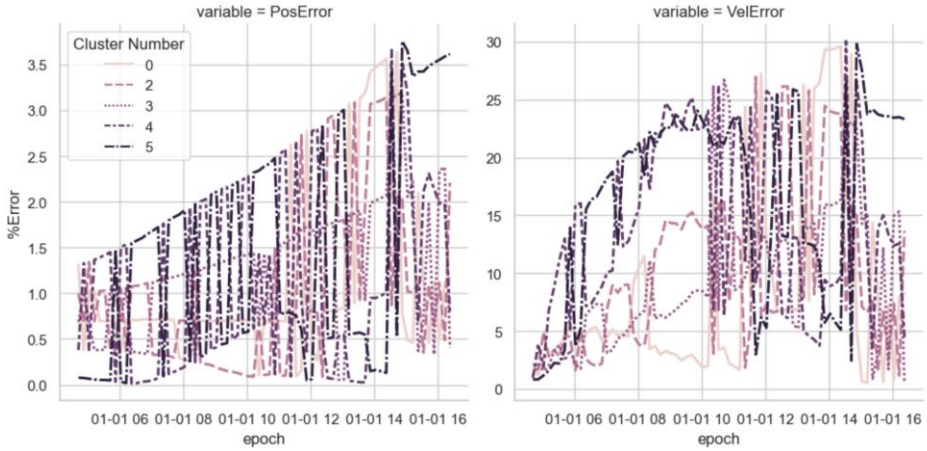


Fig. 9. Position and Velocity Errors for Three-Station TDOA (3TDOA)

In Fig. 9, the average percent error results for Three-Station TDOA (3TDOA) show a large amount of variability between the five clusters in terms of position and velocity percent error. The entropy for this case is also the highest of any presented cases, which was not surprising based on our experience working with TDOA and OWD data. Over this timescale, the entropy is very slowly decreasing. This means it is still likely that the PGMF will converge, it will just take longer with the TDOA phenomenology than for the other phenomenologies explored here.

### 5.2.5 Three-Station TDOA Fused with Single-Station OWD

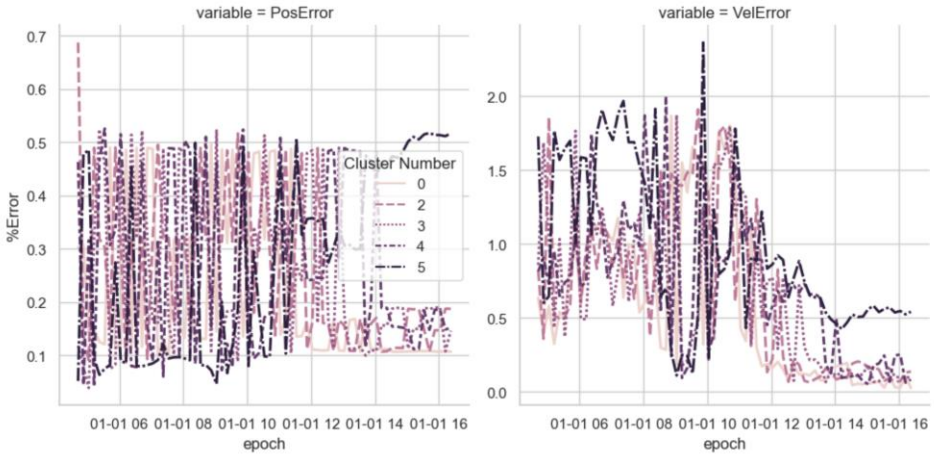


Fig. 10. Position and Velocity Errors for 3TDOA Fused with 1OWD.

Fig. 10 displays results from a simulation using the practical combination of 1OWD and 3TDOA. There is a distinct reduction in percent position and velocity errors, and a swift convergence in the velocity error. This is a promising result, as these two passive RF data types are commonly available.

### 5.2.6 Three-Station TDOA Fused with Three-Station OWD

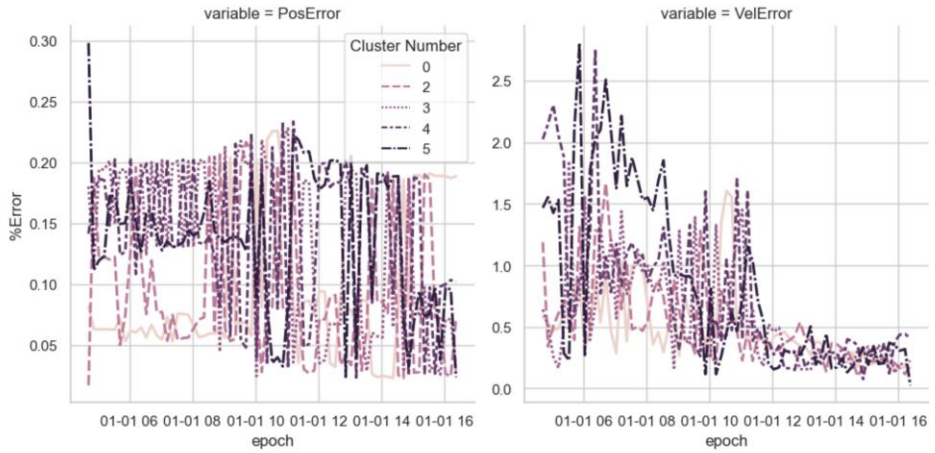


Fig. 11. Position and Velocity Errors for 3TDOA Fused with 3OWD.

Fusing the two types of RF measurements, TDOA and 3OWD, in Fig. 11 shows a swift downward trend in the percent error in position and velocity. These results are similar to the lower-information results from the combination of 3TDOA and 1OWD, though this version converges faster (as may be expected), and the entropy results are nearly the same.

## 5.3 EO-RF Fusion case

### 5.3.1 Electro-Optical Fused with Three-Station TDOA and Three-Station One-Way Doppler

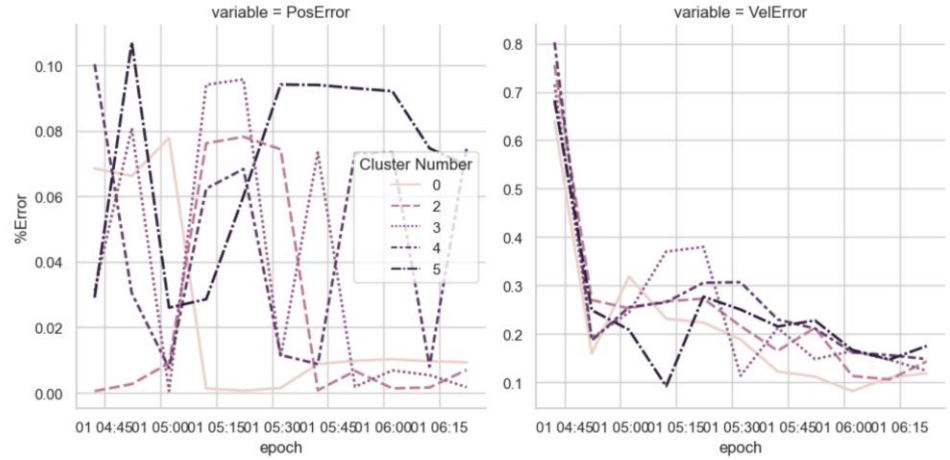


Fig. 12. Position and Velocity Errors for a Combination of All Three Measurement Types: EO, 3TDOA and 3OWD.

When all the measurement types available are used in one simulation, as shown in Fig. 12, the filter converges extremely quickly to lower errors in position and velocity accuracy. If available, both EO and RF together make an excellent combination for performing OD with the PGMF.

In cislunar space, with the spacecraft approximately 3,000,000 km distance from the ground-based sensors here, a 0.1% position and 0.15% velocity average error are quite remarkable. That means the estimated state of the highly nonlinear dynamical system is only about 300 km and 1.2 m/s different than the true state after 16 hours. This result may enable highly accurate OD processing of incredibly far-away objects.

### 5.4 Comparison in Terms of Entropy

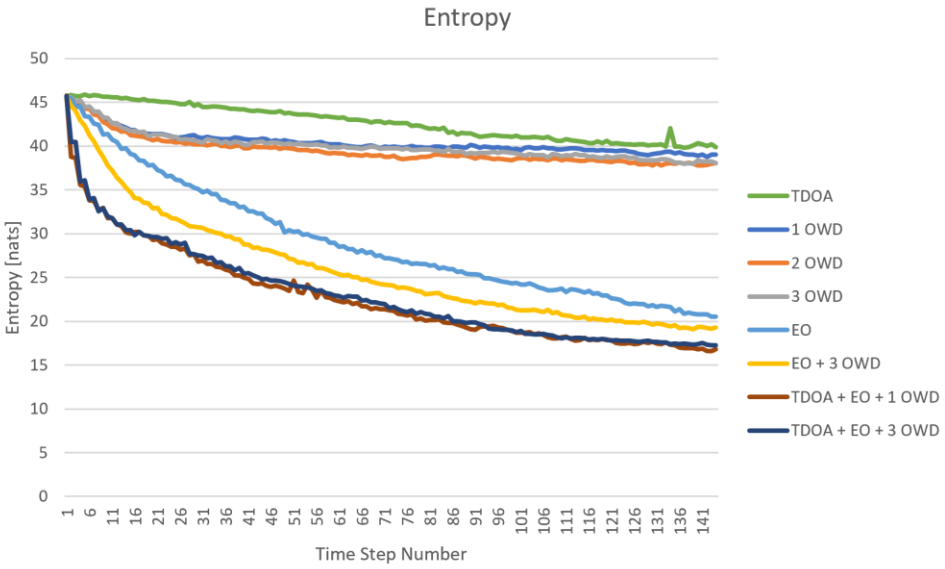


Fig. 13. Entropy, as Produced by the PGMF, Over Time for All Cases.

Fig. 13 shows the entropy over time for each of the cases listed in the previous sections. We have the following observations:

- We look to EO-only as the baseline performance, shown in light blue in Fig. 13. We notice here that with every additional EO observation we get a pronounced drop in entropy, shown in the figure as a consistent decrease in entropy values. We believe that at some point, the EO entropy plot will flatten out as uncertainty in the track of the target approaches the uncertainty contained in the observed data determined by the sensor noise characteristics.
- This plateau effect is more pronounced in the TDOA-only and OWD-only entropy plots (top four lines in Fig. 13) since the informational return from a single passive RF collection is not as large as that of EO observations.
- TDOA and OWD, or the RF data types in general, perform worst when they are used on their own without fusion with EO data.
- TDOA-only (the green line) performs worse than OWD-only (orange, gray and medium dark blue lines in the figure) even for a single-station OWD.
- Fusing TDOA and OWD together yields lower entropy (i.e., improved performance) over time, but it is still high compared to EO alone.
- Adding passive RF observations to EO observations is valuable in reducing the target tracking uncertainty (see yellow line in the figure).
- Fusing all three measurement types provides the quickest decrease and least absolute amount of entropy.

### 5.5 Comparison of Results

By both measurements of performance – overall entropy and percentage error from truth – the fusion of EO and RF measurements yields better target tracking more quickly than either EO or RF alone. EO-only is less uncertain and more accurate than any RF-only method. Fusion is the best method for OD with RF if both TDOA and OWD are available. However, it is still possible to produce accurate, more certain target tracks with either TDOA or OWD observations alone. More measurements over longer periods of time help to produce more robust information states in every case.

## 6. CONCLUSIONS

The PAR-PGMF framework from [1] was modified to incorporate passive RF observations for orbit determination. Percent errors in position and velocity and overall entropy were used as metrics to assess and compare the OD performance of the PGMF using EO-only, RF-only, and an EO-RF fusion of observations of a satellite in a lunar resonant orbit from up to three ground sites in the Pacific Ocean. OWD and TDOA observations provide sufficient information to provide state updates to a target, and although not as beneficial as EO-only, do provide complementary information to EO that could help maintain target tracking, especially through periods of EO observation outages. Fusing RF with EO shows promise, with a faster drop in entropy, which results in less uncertainty in the target's propagated state. In future work, we will assess filter performance over longer periods of time, where in some cases, the EO and RF observations appear and drop as the geometry between the ground stations and target evolves. We anticipate that the fused EO-RF PGMF should be more robust to observation outages than any single observation alone.

## 7. REFERENCES


[1] M. Bolden, I. Hussein, H. Borowski , R. See and E. Griggs, "Probabilistic Initial Orbit Determination and Object Tracking in Cislunar Space Using Optical Sensors," in *AMOS*, Wailea, HI, 2022.

[2] United States Space Force, Spacepower: Doctrine for Space Forces. Nimble Books, 2020.

[3] I. Hussein, C. W. T. Roscoe, M. Mercurio, M. P. Wilkins and P. W. Schumacher, Jr., "Probabilistic Admissible Region for Multi-Hypothesis Filter Initialization," *J. Guidance, Control and Dynamics,*, vol. 41, no. 3, 2017.

[4] D. Raihan and S. Chakravorty, "Particle Gaussian Mixture Filters I," *Automatica*, vol. 98, pp. 331-340, 2018.

[5] D. Raihan and S. Chakravorty, "Particle Gaussian Mixture Filters II," *Automatica*, vol. 98, pp. 341-348, 2018.

[6] A. Gelb, Applied Optimal Estimation., MIT Press, 1974.

[7] R. Ludwig and J. Taylor, "Voyager Telecommunications," Jet Propulsion Laboratory, Pasadena, CA, 2002.

[8] P. Misra and P. Enge, Global Positioning System: Signals Measurements, and Performance Revised Second Edition, Lincoln, MA: Ganga-Jamuna Press, 2011.

[9] T. Bengtsson, P. Bickel and B. Li, "Curse-of-dimensionality revisited: Collapse of particle filter in very large-scale systems," *Probability and Statistics: Essays in Honor of David A. Freedman*, vol. 2, p. 316–334, 2008.

[10] T. Kelecy, M. Jah and K. DeMars, "Application of a Multiple Hypothesis Filter to near GEO high area-to-mass ratio space objects state estimation," *Acta Astronautica*, vol. 81, pp. 435-444, 2012.

[11] M. D. Hejduk, "Specular and Diffuse Components in Spherical Satellite Photometric Modeling," in *AMOS*, Wailea, HI, 2011.

[12] V. Szebehely, Theory of Orbits: The Restricted Problem of Three Bodies, New York : Academic Press, 1967.

[13] S. P. Lloyd, "Least squares quantization in pcm," *IEEE Transactions on Information Theory*, vol. 28, no. 1, p. 129–137, 1982.

[14] A. K. Jain, M. N. Murty and P. J. Flynn, "Data clustering: a review," *ACM Computing Surveys*, vol. 31, no. 3, p. 264–323, 1999.

[15] D. Adamy, in *EW 101: A First Course in Electronic Warfare*, Norwood, MA, ARTECH HOUSE, INC., 2001, pp. 172-176.

[16] International Telecommunication Union, "SNL Online," 2023. [Online]. Available: https://www.itu.int/snl/freqtab_snl.html.

[17] Federal Communications Commission, "FCC Frequency Assignment Databases," 3 August 2016. [Online]. Available: https://www.fcc.gov/fcc-frequency-assignment-databases.